High-Energy Collision of Quarks and Mesons in the Schwinger Model: From Tensor Networks to Circuit QED

Ron Belyansky,[1,2,*] Seth Whitsitt,[1,2] Niklas Mueller,[3] Ali Fahimniya,[1,2] Elizabeth R. Bennewitz,[1,2] Zohreh Davoudi,[4,1] and Alexey V. Gorshkov[1,2]

[1]*Joint Center for Quantum Information and Computer Science, NIST/University of Maryland, College Park, Maryland 20742 USA*
[2]*Joint Quantum Institute, NIST/University of Maryland, College Park, Maryland 20742 USA*
[3]*InQubator for Quantum Simulation (IQuS), Department of Physics, University of Washington, Seattle, Washington 98195, USA*
[4]*Maryland Center for Fundamental Physics and Department of Physics, University of Maryland, College Park, Maryland 20742 USA*

(Received 2 August 2023; revised 23 December 2023; accepted 23 January 2024; published 28 February 2024)

With the aim of studying nonperturbative out-of-equilibrium dynamics of high-energy particle collisions on quantum simulators, we investigate the scattering dynamics of lattice quantum electrodynamics in $1+1$ dimensions. Working in the bosonized formulation of the model and in the thermodynamic limit, we use uniform-matrix-product-state tensor networks to construct multiparticle wave-packet states, evolve them in time, and detect outgoing particles post collision. This facilitates the numerical simulation of scattering experiments in both confined and deconfined regimes of the model at different energies, giving rise to rich phenomenology, including inelastic production of quark and meson states, meson disintegration, and dynamical string formation and breaking. We obtain elastic and inelastic scattering cross sections, together with time-resolved momentum and position distributions of the outgoing particles. Furthermore, we propose an analog circuit-QED implementation of the scattering process that is native to the platform, requires minimal ingredients and approximations, and enables practical schemes for particle wave-packet preparation and evolution. This study highlights the role of classical and quantum simulation in enhancing our understanding of scattering processes in quantum field theories in real time.

DOI: 10.1103/PhysRevLett.132.091903

Introduction.—Scattering processes in nuclear and high-energy physics play an essential role in studies of fundamental particles and interactions. Current and future frontiers in scattering experiments are the Large Hadron Collider, the Relativistic Heavy-Ion Collider [1,2], the Electron-Ion Collider [3,4], and the Deep Underground Neutrino Experiment [5–8]. Collisions in these experiments involve hadronic initial states and complex many-particle final states. The scattering proceeds in a multistage process and may encompass a wide range of phenomena, including the formation of exotic matter [2,9], such as quark-gluon plasma [10,11], thermalization [12,13], fragmentation [14,15], and hadronization [16,17]. Ideally, such phenomenology should be grounded in first-principles quantum-chromodynamics (QCD) descriptions. While perturbation theory and QCD factorization [18–21], as well as lattice QCD [22–30], have brought about impressive advances, a full understanding of scattering processes in QCD is still lacking. In particular, lattice-QCD studies of hadronic scattering based on Monte Carlo methods in Euclidean spacetime have so far been limited to low energy and low inelasticities [31,32]. These also do not track the state evolution after the collision.

First-principles simulations of high-energy particle scattering are a prime application for quantum simulators [33–44]. However, realistic experiments involve a vast range of spatial and temporal scales, placing their simulation beyond the capabilities of current digital quantum computers. Analog quantum simulators may enable simulating larger Hilbert spaces and longer times, but concrete proposals for simulating scattering processes in quantum field theories are lacking. At the same time, classical tensor-network methods have been shown to successfully capture ground-state [45], and to some degree dynamical [46], phenomena in gapped theories, including scattering processes [47–50], particularly in $1+1$ dimensions, but their reach remains limited in simulating general scattering problems in quantum field theories. This manuscript advances both analog quantum simulation and tensor-network-based classical simulation for a prototypical model of QCD, the lattice Schwinger model, i.e., lattice quantum electrodynamics (QED) in $1+1$ dimensions. Previous tensor-network [47,48,51–62] and quantum-simulation [63–88] studies of the model focused on formulations involving fermion (or qubit) degrees of freedom (with or without gauge fields). Motivated to address, more generally, theories with bosonic content, here we instead consider the bosonic dual of the theory, a particular type of a massive sine-Gordon model.

Our first objective is a numerical exploration of high-energy real-time scattering phenomenology in the model. We work in the nonperturbative regime, near the

confinement-deconfinement critical point and in the thermodynamic limit, using uniform matrix product states (uMPS) [89], which allows for the construction [49,50] and collision of numerically exact quasiparticle wave packets in the interacting theory at various energies, resulting in nontrivial inelastic effects. In contrast, earlier works were limited to elastic scattering at either weak (nearly free fermions) [48] or strong (nearly free bosons) [47] coupling regimes. We focus on spatial, temporal, and momentum-resolved diagnostics of elastic and inelastic processes of quark and meson states, involving phenomena such as meson disintegration, dynamical string formation and breaking, and the creation of quark and (excited) meson states. We also investigate the role of entanglement in high-energy scattering [47,90–97]. Our second objective is to propose an analog circuit-QED implementation of the bosonized lattice Schwinger model. Recently, the bosonic dual was shown to be approximately realizable by circular Rydberg states [98]. In contrast, we will show that circuit QED's basic components, its native bosonic degrees of freedom, and the available ultrastrong coupling [99,100] allow the model to be implemented in a simple circuit with minimal ingredients and approximations, making it particularly suitable for near-term quantum simulation that goes beyond the classical simulation methods.

Model.—The massive Schwinger model has the Lagrangian density

$$\mathcal{L} = \bar{\psi}\left(i\gamma^\mu \partial_\mu - e\gamma^\mu A_\mu - m\right)\psi - \frac{1}{4}F_{\mu\nu}F^{\mu\nu}, \tag{1}$$

where $\psi(x,t)$ is a two-component Dirac spinor, $\gamma^0 = \sigma^z$, $\gamma^1 = i\sigma^y$ with σ^z, σ^y being the Pauli matrices, m is the mass, e is the electric charge, and $A_\mu(x,t)$ and $F_{\mu\nu}(x,t)$ are the gauge field and the field-strength tensor, respectively. Equation (1) is dual to a bosonic scalar field theory with the Hamiltonian [101,102]

$$H = \int dx : \left[\frac{\Pi^2}{2} + \frac{(\partial_x\phi)^2}{2} + \frac{e^2\phi^2}{2\pi} - \frac{b\,m\,e\cos(\sqrt{4\pi}\phi - \theta)}{2\pi^{3/2}}\right] :, \tag{2}$$

where normal ordering $(::)$ is with respect to $e/\sqrt{\pi}$, $\phi(x)$ and $\Pi(x)$ are the scalar field and conjugate momentum, respectively, $b = \exp(\gamma)$ with γ being Euler's constant, and $\theta \in (-\pi, \pi]$, with its origin explained in Ref. [102] and the Supplemental Material [103] (we assume $\hbar = c = 1$ throughout, where c is the speed of light). We work with a lattice regularization of Eq. (2) given by

$$H = \chi \sum_x \left[\frac{\pi_x^2}{2} + \frac{(\phi_x - \phi_{x-1})^2}{2} + \frac{\mu^2\phi_x^2}{2} - \lambda\cos(\beta\phi_x - \theta)\right], \tag{3}$$

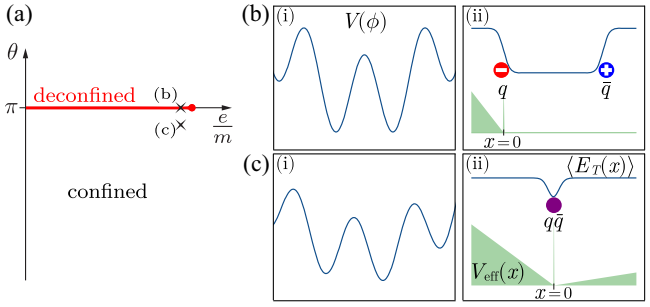

FIG. 1. (a) Sketch of the phase diagram of the massive Schwinger model as a function of e/m (corresponding to μ/λ) and θ. The red dot is the Ising critical point, where the deconfined phase (red line) terminates. Points (b) and (c) correspond to the two regimes considered in the main text. Panels (b-i) and (c-i) show the corresponding scalar potential $V(\phi) = \frac{1}{2}\mu^2\phi^2 - \lambda\cos(\sqrt{4\pi}\phi - \theta)$ [Eq. (3)]. Panels (b-ii) and (c-ii) show both the effective potential between the quarks [Eq. (4)] (green) and the electric or scalar-field distributions (blue) due to the quarks and mesons.

where x labels lattice sites, $[\phi_x, \pi_y] = i\delta_{xy}$, $\chi = 1/a$, $\beta = \sqrt{4\pi}$, $\mu^2 = a^2e^2/\pi$, $\lambda = a^2 b\,m\,e\,\exp[2\pi\Delta(a)]/2\pi^{3/2}$, a is the lattice spacing, and $\Delta(a)$ is the lattice Feynman propagator at the origin [113,114]. We set $a = 1$, with the continuum limit corresponding to $\mu, \lambda \to 0$. Quantities are assumed in lattice units throughout.

To gain insight into the anticipated phenomenology, we proceed with a numerical study of the collision dynamics in the lattice Schwinger model. While quantitative predictions for the continuum theory require an extrapolation procedure [58,115], here only fixed, but sufficiently small, values of μ and λ are considered. The model has two dimensionless parameters, the ratio e/m, corresponding to μ/λ in Eq. (3), and the angle θ representing a constant background electric field $E_\theta = (e/2\pi)\theta$. Gauss's law, $\partial_x E = e\psi^\dagger\psi$, ties the total electric field $E_T = E_\theta + E$ to the dynamical charges, and equals $E_T = (e/\sqrt{\pi})\phi$ in the bosonic dual [116].

We study two regimes near the $\mathbb{Z}_2$ critical point, shown in Fig. 1 as (b) and (c). Point (b) is in the deconfined phase [red line at $\theta = \pi$ in Fig. 1(a) terminating at the Ising critical point], where the ground state is twofold degenerate [Fig. 1(b-i)]. Here, fundamental excitations are "half-asymptotic" [102] fermions ("quarks"), appearing as topological kinks in the bosonic dual [see Fig. 1(b-ii)]. Point (c) in Fig. 1(a) is in the confined phase, with a unique ground state [Fig. 1(c-i)] and quark-antiquark bound-state ("meson") excitations.

Quark-antiquark scattering.—Constructing a uMPS representation of the two ground states [117] in the deconfined phase [Fig. 1(b)], we use the uMPS quasiparticle ansatz [118,119] to obtain single-particle energy-momentum eigenstates with dispersion $\mathcal{E}(p)$ and momenta $p \in [-\pi, \pi)$ [103]. From this, we construct two Gaussian wave packets, localized

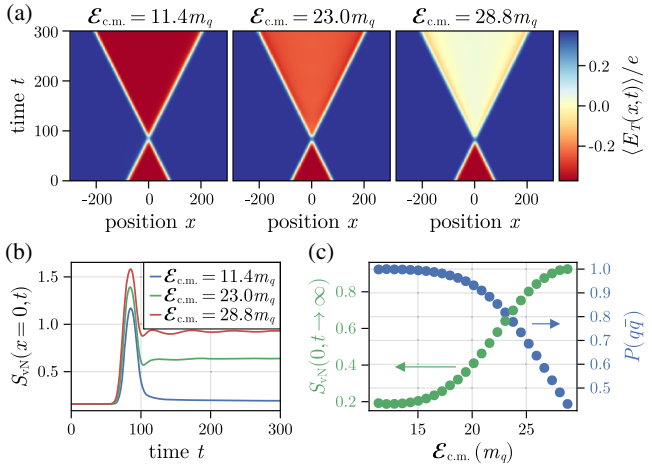

FIG. 2. Quark-antiquark scattering in the deconfined phase. (a) Time evolution of the electric field for different center-of-mass energies. (b) Time evolution of the von Neumann entanglement entropy for a cut at $x = 0$, for the same three collisions as in (a). (c) Elastic scattering probability (right, blue) and asymptotic von Neumann entanglement entropy for the $x = 0$ cut (left, green) as a function of the center-of-mass energy. The parameters are $\mu^2 = 0.1$ and $\lambda = 0.5$ [see Eq. (3)].

in momentum and position space, centered at opposite momenta $\pm p_0$. The initial state consists of a finite nonuniform region of 150 to 300 sites containing the two wave packets, and is surrounded by the uniform vacuum [we choose the vacuum with positive E_T, i.e., the right minimum of Fig. 1(b-i)]. We then time evolve this state under the Hamiltonian in Eq. (3), while dynamically expanding the nonuniform region [120–122] up to 600 to 1300 sites (see Supplemental Material [103]). By working near the critical point, where the quark mass $m_q \equiv \mathcal{E}(p = 0)$ is small, one can consider momenta up to $|p_0| \lesssim 0.8$. These are sufficiently small to keep the physics in the long-wavelength regime of the lattice model, where the dispersion is approximately relativistic $\mathcal{E}(p) \approx (p^2 + m_q^2)^{\frac{1}{2}}$, but highly relativistic center-of-mass (c.m.) energies $\mathcal{E}_{\rm c.m.} \equiv 2\mathcal{E}(p_0) \lesssim 30m_q$ are achieved.

Figure 2(a) shows the space-time distribution of the electric field for collisions at three representative energies, $\mathcal{E}_{\rm c.m.}/m_q = 11.4$, 23.0, and 28.8. Initially, the quark and antiquark are separated, resembling Fig. 1(b-ii), with electric field between the charges equal in magnitude but opposite in sign to the field outside [the two regions correspond to the two degenerate ground states in Fig. 1(b-i)]. Under time evolution, the two charges propagate ballistically, shrinking the negative-field region until they collide. During the collision, the particles bounce off each other and reverse their propagation direction elastically, the sole process at lower energies. Specifically, as can be seen in Fig. 2(a), at the lowest energy, $\mathcal{E}_{\rm c.m.}/m_q = 11.4$, the postcollision value of E_T between the charges is practically equal to the pre-collision value. For the higher-energy collisions, $\mathcal{E}_{\rm c.m.}/m_q = 23.0$ and 28.8, an increase of the postcollision electric field is observed, signaling additional charge production.

While our numerical approach does not rely on strong- or weak-coupling expansion, the relevant scattering channels can be understood from weak-coupling arguments as follows. In the Supplemental Material [103], we derive, in the nonrelativistic limit, an effective potential between opposite charges at the lowest order in e/m starting from Eq. (1), which reads (in the center-of-mass frame)

$$V_{\rm eff}(x) = \frac{e^2}{2}\left(|x| - \frac{\theta}{\pi}x\right) + \frac{e^2}{4m^2}\delta(x). \tag{4}$$

Here, x is the distance between charges. For $\theta \neq \pi$, one recovers linear confinement [Fig. 1(c-ii)] [52,102,116,123], while at $\theta = \pi$, charges experience short-range *repulsion* due to the delta function in Eq. (4) [Fig. 1(b-ii)]. This implies the absence of stable bound states (mesons) in the deconfined phase, which is confirmed numerically in the Supplemental Material [103]. All possible scattering channels are, therefore, (even-numbered) multiquark states. The lowest-order inelastic channel is the four-quark production ($q\bar{q} \to q\bar{q}q\bar{q}$), exhibiting quark fragmentation. The two inner particles screen the electric field produced by the outer two, consistent with the two rightmost panels in Fig. 2(a).

Elastic and inelastic processes are also distinguished by the von Neumann entanglement entropy [124] across the collision point ($x = 0$), shown in Fig. 2(b) as a function of time. Figure 2(c) also shows the asymptotic ($t \to \infty$) entanglement as a function of the collision energy. The entanglement is maximal during the collision but quickly approaches a constant afterwards. At lower energies, it nearly returns to its precollision (vacuum) value. A small increase is observed because different momentum components of the wave packets acquire slightly different elastic scattering phase shifts [50]. At higher energies, however, significant net entanglement is generated, indicating inelastic particle production [34].

Finally, we compute elements of the momentum-resolved scattering S matrix by projecting the postcollision state onto a basis of asymptotic two-particle states (see Supplemental Material [103]). This basis is constructed from the single-particle wave functions, requiring the particles to be widely separated to ensure orthogonality and avoid interaction effects. For $2 \to 2$ scattering, this is guaranteed sufficiently far from the collision point. From this, we obtain the elastic scattering probability $P(q\bar{q})$, displayed in Fig. 2(c), as a function of the collision energy.

The elastic scattering probability is near unity at lower energies, decreasing monotonically, falling below 0.5 around $\mathcal{E}_{\rm c.m.}/m_q \gtrsim 28$. Interestingly, the energy required for significant inelastic scattering is many times the threshold energy ($\mathcal{E}_{\rm c.m.} = 4m_q$). While we did not obtain the

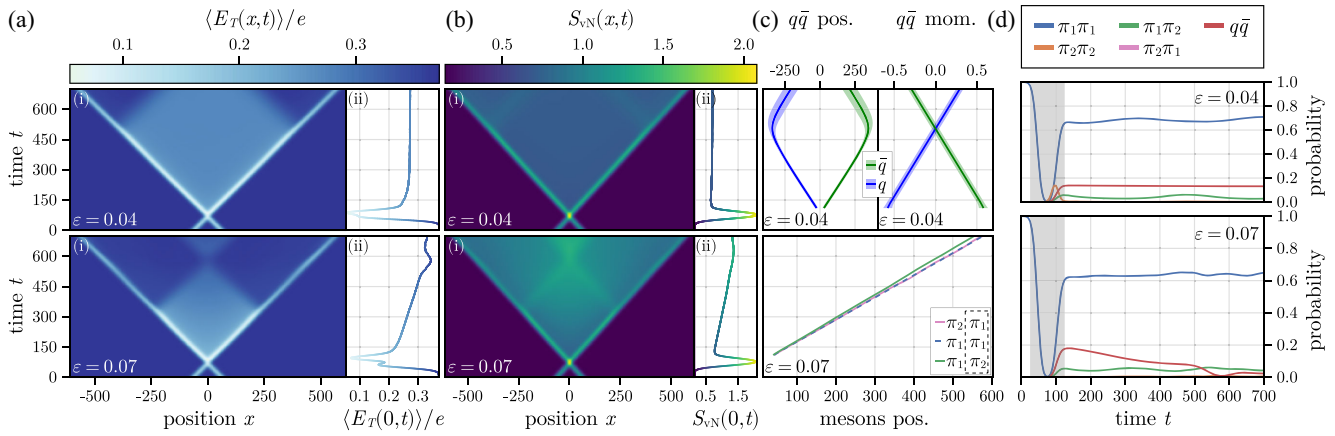

FIG. 3. Meson-meson scattering in the confined phase. (a) Time evolution of the electric field for different $\theta = \pi - \varepsilon$ at all positions x [panels (i)] and at $x = 0$ [panels (ii)] with $\mu^2 = 0.1$ and $\lambda = 0.5$ as in Fig. 2. The wave packets are centered at $p_0 = \pm 0.6$, corresponding to $\mathcal{E}_{\text{c.m.}}/m_{\pi_1} = 6.84, 5.95$ for $\varepsilon = 0.04, 0.07$. (b) Time evolution of the von Neumann entanglement entropy at all positions x [panels (i)] and at $x = 0$ [panels (ii)]. (c) Momenta and positions (mean $\pm$ std. extracted from a Gaussian fit of the projected distributions) of the quarks for $\varepsilon = 0.04$ (top) and the mean positions of the right-moving mesons for $\varepsilon = 0.07$ (bottom). (d) Probabilities of two-particle states $\mu\nu$ ($\mu, \nu \in [\pi_1, \pi_2, q, \bar{q}]$), where $\mu(\nu)$ is the particle on the left (right). The curves for $\pi_1\pi_2$ and $\pi_2\pi_1$ overlap due to the reflection symmetry of the initial state. Near the initial collision (shaded region), and the secondary collision at $t \approx 550$ for $\varepsilon = 0.07$, the state cannot be fully captured by a basis of asymptotic particles.

precise contribution of the four-quark (or higher-quark-number) states [125], the decrease of $P(q\bar{q})$ confirms the presence of significant inelastic scattering, consistent with the increase in entanglement in Fig. 2(b) and the screening of E_T in Fig. 2(a).

Meson-meson scattering.—We next choose $\theta = \pi - \varepsilon$ with $\varepsilon \ll 1$, which gives rise to weak confinement of quarks, but keeps us close to the critical point (all other parameters are unchanged). In contrast to the deconfined regime, the interplay of high-energy and weak confinement yields rich behavior following the collision. There are multiple stable scalar meson excitations, which are labeled by $\pi_j (j = 1, 2, \ldots)$, with increasing masses m_{π_j}. Here, we consider $\pi_1\pi_1$ collisions, with meson wave packets prepared similarly as before, centered at $p_0 = \pm 0.6$ with $\mathcal{E}_{\text{c.m.}}/m_{\pi_1} = 6.84$ (5.95) for $\varepsilon = 0.04$ (0.07).

The electric-field evolution for the two collisions is displayed in Fig. 3(a-i). Before the collision, the background electric field is only locally disturbed by the charge-neutral mesons [Fig. 1(c-ii)]. After the collision, the mesons partially fragment into a quark-antiquark pair. The quarks are joined by an electric-field string which screens the background electric field (light-blue regions) inside the collision cone. As the quarks travel outward, their kinetic energy gets converted into the potential energy of the string. Eventually, they turn and propagate back in the opposite direction [see also Fig. 3(c)] causing a second collision. Weaker confinement $\varepsilon = 0.04$ allows the quarks to propagate farther.

Next, we project the time-evolved state onto two-particle components, focusing on the lightest two mesons π_1, π_2, and the quark-antiquark pair $q\bar{q}$. While the latter are not true (i.e., asymptotic) quasiparticles, at weak confinement $\varepsilon \ll 1$, (anti)quarks can be approximately described by the modified quasiparticle ansatz of Ref. [50]. This requires a uMPS representation of the electric-flux string, which we approximate by its lowest energy state, a so-called "false-vacuum" state [126,127], corresponding to the second (local) minimum in Fig. 1(c-i).

Figure 3(d) shows the probabilities of the $\pi_1\pi_1$, $\pi_2\pi_2$, $\pi_1\pi_2$, $\pi_2\pi_1$, and $q\bar{q}$ states [where in state $\mu\nu$, the particle $\mu(\nu)$ is on the left (right)]. One can observe significant flavor-conserving elastic scattering, $\pi_1\pi_1 \to \pi_1\pi_1$, a smaller probability of exciting one of the outgoing mesons, $\pi_2\pi_1$ and $\pi_1\pi_2$, and a substantial $q\bar{q}$ component. Interestingly, for $\varepsilon = 0.07$, the $q\bar{q}$ component is decreasing in time, indicating string breaking [52,128], which is also visible in the gradual increase of the bipartite entanglement entropy in Fig. 3(b-i) [see also Fig. 3(b-ii)], and in the gradual reduction of the electric-field screening [Fig. 3(a-ii)]. At a late time $t = 700$, asymptotic two-particle states (including the quark-antiquark state) account for about 90% (76%) of the state at $\varepsilon = 0.04$ (0.07) [129].

The projection onto the asymptotic two-particle basis also provides the full momentum, and, consequently, position, distributions of the particles. Figure 3(c) shows the mean and standard deviation of the positions and momenta of the quarks, and the mean positions of the mesons, computed from fits of these distributions to a Gaussian form. The mean momenta of the quarks are approximately $\langle p(t)\rangle \propto \pm t$, in agreement with the expectation from the linear potential of Eq. (4). Their extracted positions in Fig. 3(c) are consistent with the boundaries of the screened-field region in Fig. 3(a-i) and with the

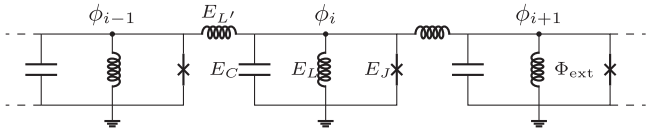

FIG. 4. Lumped-element circuit diagram that realizes Eq. (3).

localized increase in the entanglement entropy in Fig. 3(b-i). From the mean position of the mesons, Fig. 3(c), one can see that the heavier meson π_2 has a slightly lower average velocity compared to π_1, as expected.

Circuit-QED implementation.—The increasingly large entanglement production occurring with higher-energy collisions (Fig. 2) or stronger confinement and longer collision times (Fig. 3) limits the regimes of applicability of the MPS-based methods. This motivates the use of quantum simulators as an alternative approach, which is expected to evade such limitations. Remarkably, the lattice Schwinger Hamiltonian [Eq. (3)] can be exactly realized in a simple superconducting circuit, shown in Fig. 4. The circuit can be regarded as a chain of inductively coupled fluxoniums [130]. It consists of nodes i, each corresponding to a lattice site with a local bosonic degree of freedom described by flux ϕ_i and charge π_i, composed of a parallel arrangement of a capacitor, an inductor, and a Josephson junction with respective energies E_C, E_L, and E_J [131]. Nodes are coupled by inductors with energy $E_{L'}$. The circuit parameters are related to those of Eq. (3) via $\chi = (8E_C/\beta^2)$, $(E_{L'}\beta^4/8E_C) = 1$, $\mu^2 = (E_L\beta^4/8E_C)$, $\lambda = (E_J\beta^2/8E_C)$, and $\theta = \Phi_{\text{ext}} - \pi$, where Φ_{ext} is a tunable external flux threading each loop, and $\beta \neq 0$ can be chosen arbitrarily (see Supplemental Material [103]). In fact, when $\beta \neq \sqrt{4\pi}$, the circuit describes a more general model known as the massive Thirring-Schwinger model [132]. In the Supplemental Material [103], we present a method for preparing initial wave packets of bosonic particles using two ancillary qubits, hence providing a complete protocol for preparation and evolution of mesonic wave packets for a scattering experiment. Measurements of the local density [133] or the output field at the edges [134,135] can be performed using standard techniques.

Discussion and outlook.—Using *ab initio* numerical uMPS computations and working with a bosonized formulation of the Schwinger model, we analyzed the real-time dynamics of high-energy particle scattering in the nonperturbative regime of QED in $1+1$ dimensions. We also proposed an analog circuit-QED implementation of the bosonized Schwinger model. This implementation requires minimal ingredients and no approximations (besides a lattice discretization), in contrast to previous circuit-QED proposals based on a quantum-link model [85]. We studied both the confined and deconfined regimes of the model, exhibiting a multitude of phenomena, including inelastic particle production, meson disintegration, and dynamical string formation and breaking.

The single-particle excitations allowed us to obtain complete time-resolved momentum and position distributions of the outgoing $2 \to 2$ scattered particles. To account for higher-order scattering it appears necessary to include states where two particles can be close, which could potentially be accomplished using the two-particle uMPS ansatz from Ref. [136]. This might also shed light on the nontrivial transient dynamics in Fig. 3(d). It would also be interesting to explore the string dynamics more systematically [137]. Additionally, it will be valuable to investigate how other nonequilibrium phenomena, such as dynamical quantum phase transitions (DQPTs) [66,138], weak ergodicity breaking, and quantum many-body scars [139,140], can be probed in scattering processes.

In addition to exploring scattering in regimes inaccessible to the MPS methods, our circuit-QED implementation can also be used to study quench dynamics. For example, the Schwinger mechanism or DQPTs can be studied in quenches of the θ parameter [66,138], which can be accomplished using time-dependent flux control [131].

Finally, our circuit-QED implementation applies to other bosonic theories [141–144], including the ϕ^4 theory (achieved in the $\beta \to 0$ limit) in $1+1$ or $2+1$ dimensions [103] and generalizations of the bosonized Schwinger model, including to multiflavor fermions [102,145] and to Thirring interactions [132]. In the latter case, sufficiently strong Thirring interactions give rise to attractive short-range interactions between quarks in the deconfined phase, as shown in the Supplemental Material [103], leading to stable meson particles and hence qualitatively different scattering dynamics.

We acknowledge valuable discussion with A. Milsted and Z. Minev. The uMPS simulations were performed with the help of the MPSKit.jl JULIA package [146]. We thank M. Van Damme for help with the package. The authors acknowledge the University of Maryland's supercomputing resources [147] made available for conducting the research reported in this paper. R. B., S. W., A. F., and A. V. G. were supported in part by the National Science Foundation (NSF) Quantum Leap Challenge Institute (Grant No. OMA-2120757), Department of Energy (DOE), Office of Science, Office of Advanced Scientific Computing Research (ASCR), Accelerated Research in Quantum Computing program (Award No. DE-SC0020312), ARO MURI, the DOE ASCR Quantum Testbed Pathfinder program (Awards No. DE-SC0019040 and No. DE-SC0024220), NSF STAQ program, AFOSR, AFOSR MURI, and DARPA SAVaNT ADVENT. Support is also acknowledged from the DOE, Office of Science, National Quantum Information Science Research Centers, Quantum Systems Accelerator. N. M. acknowledges funding by the U.S. Department of Energy, Office of Science, Office of Nuclear Physics, InQubator for Quantum Simulation (IQuS) under Award No. DOE (NP)

Award No. DE-SC0020970 via the program on Quantum Horizons: QIS Research and Innovation for Nuclear Science. Z. D. and N. M. acknowledge funding by the DOE, Office of Science, Office of Nuclear Physics via the program on Quantum Horizons: QIS Research and Innovation for Nuclear Science (Award No. DE-SC0021143). Z. D. further acknowledges support by the DOE, Office of Science, Early Career Award (Award No. DESC0020271). E. R. B acknowledges support from the DOE, Office of Science, Office of ASCR, Computational Science Graduate Fellowship (Award No. DE-SC0023112).

*rbelyans@umd.edu

[1] W. Florkowski, *Phenomenology of Ultra-Relativistic Heavy-Ion Collisions* (World Scientific, Singapore, 2010).

[2] A. Lovato, T. Dore, R. D. Pisarski, B. Schenke, K. Chatziioannou, J. S. Read, P. Landry, P. Danielewicz, D. Lee, S. Pratt, F. Rennecke, H. Elfner, V. Dexheimer, R. Kumar, M. Strickland *et al.*, Long Range Plan: Dense matter theory for heavy-ion collisions and neutron stars, arXiv:2211.02224.

[3] A. Accardi, J. L. Albacete, M. Anselmino, N. Armesto, E. C. Aschenauer, A. Bacchetta, D. Boer, W. K. Brooks, T. Burton, N. B. Chang, W. T. Deng, A. Deshpande, M. Diehl, A. Dumitru, R. Dupré *et al.*, Electron-Ion Collider: The next QCD frontier: Understanding the glue that binds us all, Eur. Phys. J. A **52**, 268 (2016).

[4] P. Achenbach, D. Adhikari, A. Afanasev, F. Afzal, C. A. Aidala, A. Al-bataineh, D. K. Almaalol, M. Amaryan, D. Androić, W. R. Armstrong, M. Arratia, J. Arrington, A. Asaturyan, E. C. Aschenauer, H. Atac *et al.*, The present and future of QCD, arXiv:2303.02579.

[5] H. Gallagher, G. Garvey, and GP. Zeller, Neutrino-nucleus interactions, Annu. Rev. Nucl. Part. Sci. **61**, 355 (2011).

[6] L. Alvarez-Ruso, M. S. Athar, M. Barbaro, D. Cherdack, M. Christy, P. Coloma, T. Donnelly, S. Dytman, A. de Gouvêa, R. Hill, P. Huber, N. Jachowicz, T. Katori, A. Kronfeld, K. Mahn *et al.*, NuSTEC White Paper: Status and challenges of neutrino–nucleus scattering, Prog. Part. Nucl. Phys. **100**, 1 (2018).

[7] A. S. Kronfeld, D. G. Richards, W. Detmold, R. Gupta, H.-W. Lin, K.-F. Liu, A. S. Meyer, R. Sufian, and S. Syritsyn, Lattice QCD and neutrino-nucleus scattering, Eur. Phys. J. A **55**, 1 (2019).

[8] L. A. Ruso, A. M. Ankowski, S. Bacca, A. B. Balantekin, J. Carlson, S. Gardiner, R. Gonzalez-Jimenez, R. Gupta, T. J. Hobbs, M. Hoferichter, J. Isaacson, N. Jachowicz, W. I. Jay, T. Katori, F. Kling *et al.*, Theoretical tools for neutrino scattering: Interplay between lattice QCD, EFTs, nuclear physics, phenomenology, and neutrino event generators, arXiv:2203.09030.

[9] A. Sorensen, K. Agarwal, K. W. Brown, Z. Chajecki, P. Danielewicz, C. Drischler, S. Gandolfi, J. W. Holt, M. Kaminski, C.-M. Ko, R. Kumar, B.-A. Li, W. G. Lynch, A. B. McIntosh, W. G. Newton *et al.*, Dense nuclear matter equation of state from heavy-ion collisions, Prog. Part. Nucl. Phys. **134**, 104080 (2024).

[10] S. A. Bass, M. Gyulassy, H. Stoecker, and W. Greiner, Signatures of quark-gluon plasma formation in high energy heavy-ion collisions: A critical review, J. Phys. G **25**, R1 (1999).

[11] E. V. Shuryak, Quantum chromodynamics and the theory of superdense matter, Phys. Rep. **61**, 71 (1980).

[12] R. Baier, A. H. Mueller, D. Schiff, and D. T. Son, "Bottom-up" thermalization in heavy ion collisions, Phys. Lett. B **502**, 51 (2001).

[13] J. Berges, M. P. Heller, A. Mazeliauskas, and R. Venugopalan, QCD thermalization: *Ab initio* approaches and interdisciplinary connections, Rev. Mod. Phys. **93**, 035003 (2021).

[14] B. Andersson, G. Gustafson, G. Ingelman, and T. Sjostrand, Parton fragmentation and string dynamics, Phys. Rep. **97**, 31 (1983).

[15] B. R. Webber, A QCD model for jet fragmentation including soft gluon interference, Nucl. Phys. **B238**, 492 (1984).

[16] S. A. Bass and A. Dumitru, Dynamics of hot bulk QCD matter: From the quark-gluon plasma to hadronic freeze-out, Phys. Rev. C **61**, 064909 (2000).

[17] A. Andronic, P. Braun-Munzinger, K. Redlich, and J. Stachel, Decoding the phase structure of QCD via particle production at high energy, Nature (London) **561**, 321 (2018).

[18] J. D. Bjorken, Asymptotic sum rules at infinite momentum, Phys. Rev. **179**, 1547 (1969).

[19] D. J. Gross and F. Wilczek, Ultraviolet behavior of non-Abelian gauge theories, Phys. Rev. Lett. **30**, 1343 (1973).

[20] J. C. Collins, D. E. Soper, and G. Sterman, Factorization of hard processes in QCD, in *Perturbative QCD* (World Scientific, Singapore, 1989), pp. 1–91.

[21] J. Blümlein, The theory of deeply inelastic scattering, Prog. Part. Nucl. Phys. **69**, 28 (2013).

[22] A. S. Kronfeld, T. Bhattacharya, T. Blum, N. H. Christ, C. DeTar, W. Detmold, R. Edwards, A. Hasenfratz, H.-W. Lin, S. Mukherjee, K. Orginos, R. Brower, V. Cirigliano, Z. Davoudi, B. Jóo *et al.*, Lattice QCD and particle physics, arXiv:2207.07641.

[23] Z. Davoudi, E. T. Neil, C. W. Bauer, T. Bhattacharya, T. Blum, P. Boyle, R. C. Brower, S. Catterall, N. H. Christ, V. Cirigliano, G. Colangelo, C. DeTar, W. Detmold, R. G. Edwards, A. X. El-Khadra *et al.*, Report of the Snowmass 2021 topical group on lattice gauge theory, arXiv:2209.10758.

[24] S. R.. Beane, W. Detmold, K. Orginos, and M. J. Savage, Nuclear physics from lattice QCD, Prog. Part. Nucl. Phys. **66**, 1 (2011).

[25] Z. Davoudi, W. Detmold, P. Shanahan, K. Orginos, A. Parreno, M. J. Savage, and M. L. Wagman, Nuclear matrix elements from lattice QCD for electroweak and beyond-Standard-Model processes, Phys. Rep. **900**, 1 (2021).

[26] C. Drischler, W. Haxton, K. McElvain, E. Mereghetti, A. Nicholson, P. Vranas, and A. Walker-Loud, Towards grounding nuclear physics in QCD, Prog. Part. Nucl. Phys. **121**, 103888 (2021).

[27] H.-T. Ding, F. Karsch, and S. Mukherjee, Thermodynamics of strong-interaction matter from Lattice QCD, Int. J. Mod. Phys. E **24**, 1530007 (2015).

[28] C. Ratti, Lattice QCD and heavy ion collisions: A review of recent progress, Rep. Prog. Phys. **81**, 084301 (2018).

[29] A. Bazavov, F. Karsch, S. Mukherjee, and P. Petreczky, Hot-dense lattice QCD, Eur. Phys. J. A **55**, 194 (2019).

[30] J. N. Guenther, Overview of the QCD phase diagram: Recent progress from the lattice, Eur. Phys. J. A **57**, 136 (2021).

[31] R. A. Briceno, J. J. Dudek, and R. D. Young, Scattering processes and resonances from lattice QCD, Rev. Mod. Phys. **90**, 025001 (2018).

[32] M. T. Hansen and S. R. Sharpe, Lattice QCD and three-particle decays of resonances, Annu. Rev. Nucl. Part. Sci. **69**, 65 (2019).

[33] S. P. Jordan, K. S. M. Lee, and J. Preskill, Quantum computation of scattering in scalar quantum field theories, Quantum Inf. Comput. **14**, 1014 (2014).

[34] S. P. Jordan, K. S. Lee, and J. Preskill, Quantum algorithms for quantum field theories, Science **336**, 1130 (2012).

[35] S. P. Jordan, H. Krovi, K. S. Lee, and J. Preskill, BQP-completeness of scattering in scalar quantum field theory, Quantum **2**, 44 (2018).

[36] A. Roggero, A. C. Y. Li, J. Carlson, R. Gupta, and G. N. Perdue, Quantum computing for neutrino-nucleus scattering, Phys. Rev. D **101**, 074038 (2020).

[37] N. Mueller, A. Tarasov, and R. Venugopalan, Deeply inelastic scattering structure functions on a hybrid quantum computer, Phys. Rev. D **102**, 016007 (2020).

[38] J. Barata, N. Mueller, A. Tarasov, and R. Venugopalan, Single-particle digitization strategy for quantum computation of a ϕ^4 scalar field theory, Phys. Rev. A **103**, 042410 (2021).

[39] R. C. Farrell, I. A. Chernyshev, S. J. M. Powell, N. A. Zemlevskiy, M. Illa, and M. J. Savage, Preparations for quantum simulations of quantum chromodynamics in $1+1$ dimensions. II. Single-baryon β-decay in real time, Phys. Rev. D **107**, 054513 (2023).

[40] F. M. Surace and A. Lerose, Scattering of mesons in quantum simulators, New J. Phys. **23**, 062001 (2021).

[41] C. W. Bauer, Z. Davoudi, A. B. Balantekin, T. Bhattacharya, M. Carena, W. A. De Jong, P. Draper, A. El-Khadra, N. Gemelke, M. Hanada, D. Kharzeev, H. Lamm, Y.-Y. Li, J. Liu, M. Lukin *et al.*, Quantum simulation for high-energy physics, PRX Quantum **4**, 027001 (2023).

[42] D. Beck, J. Carlson, Z. Davoudi, J. Formaggio, S. Quaglioni, M. Savage, J. Barata, T. Bhattacharya, M. Bishof, I. Cloet, A. Delgado, M. DeMarco, C. Fink, A. Florio, M. Francois *et al.*, Quantum information science and technology for nuclear physics. Input into U.S. long-range planning, arXiv:2303.00113.

[43] N. Klco, A. Roggero, and M. J. Savage, Standard model physics and the digital quantum revolution: Thoughts about the interface, Rep. Prog. Phys. **85**, 064301 (2022).

[44] C. W. Bauer, Z. Davoudi, N. Klco, and M. J. Savage, Quantum simulation of fundamental particles and forces, Nat. Rev. Phys. **5**, 420 (2023).

[45] U. Schollwöck, The density-matrix renormalization group in the age of matrix product states, Ann. Phys. (Amsterdam) **326**, 96 (2011).

[46] S. Paeckel, T. Köhler, A. Swoboda, S. R. Manmana, U. Schollwöck, and C. Hubig, Time-evolution methods for matrix-product states, Ann. Phys. (Amsterdam) **411**, 167998 (2019).

[47] T. Pichler, M. Dalmonte, E. Rico, P. Zoller, and S. Montangero, Real-time dynamics in U(1) lattice gauge theories with tensor networks, Phys. Rev. X **6**, 011023 (2016).

[48] M. Rigobello, S. Notarnicola, G. Magnifico, and S. Montangero, Entanglement generation in $(1+1)D$ QED scattering processes, Phys. Rev. D **104**, 114501 (2021).

[49] M. Van Damme, L. Vanderstraeten, J. De Nardis, J. Haegeman, and F. Verstraete, Real-time scattering of interacting quasiparticles in quantum spin chains, Phys. Rev. Res. **3**, 013078 (2021).

[50] A. Milsted, J. Liu, J. Preskill, and G. Vidal, Collisions of false-vacuum bubble walls in a quantum spin chain, PRX Quantum **3**, 020316 (2022).

[51] B. Buyens, J. Haegeman, K. Van Acoleyen, H. Verschelde, and F. Verstraete, Matrix product states for gauge field theories, Phys. Rev. Lett. **113**, 091601 (2014).

[52] B. Buyens, J. Haegeman, H. Verschelde, F. Verstraete, and K. Van Acoleyen, Confinement and string breaking for QED 2 in the Hamiltonian picture, Phys. Rev. X **6**, 041040 (2016).

[53] B. Buyens, J. Haegeman, F. Hebenstreit, F. Verstraete, and K. Van Acoleyen, Real-time simulation of the Schwinger effect with matrix product states, Phys. Rev. D **96**, 114501 (2017).

[54] T. M. R. Byrnes, P. Sriganesh, R. J. Bursill, and C. J. Hamer, Density matrix renormalization group approach to the massive Schwinger model, Phys. Rev. D **66**, 013002 (2002).

[55] M. Bañuls, K. Cichy, J. Cirac, and K. Jansen, The mass spectrum of the Schwinger model with matrix product states, J. High Energy Phys. 11 (2013) 158.

[56] E. Rico, T. Pichler, M. Dalmonte, P. Zoller, and S. Montangero, Tensor networks for lattice gauge theories and atomic quantum simulation, Phys. Rev. Lett. **112**, 201601 (2014).

[57] M. C. Bañuls, K. Cichy, J. I. Cirac, K. Jansen, and H. Saito, Thermal evolution of the Schwinger model with matrix product operators, Phys. Rev. D **92**, 034519 (2015).

[58] K. Zapp and R. Orús, Tensor network simulation of QED on infinite lattices: Learning from $(1+1)$ d, and prospects for $(2+1)$ d, Phys. Rev. D **95**, 114508 (2017).

[59] L. Funcke, K. Jansen, and S. Kühn, Topological vacuum structure of the Schwinger model with matrix product states, Phys. Rev. D **101**, 054507 (2020).

[60] N. Butt, S. Catterall, Y. Meurice, R. Sakai, and J. Unmuth-Yockey, Tensor network formulation of the massless Schwinger model with staggered fermions, Phys. Rev. D **101**, 094509 (2020).

[61] M. C. Bañuls and K. Cichy, Review on novel methods for lattice gauge theories, Rep. Prog. Phys. **83**, 024401 (2020).

[62] Y. Meurice, R. Sakai, and J. Unmuth-Yockey, Tensor lattice field theory for renormalization and quantum computing, Rev. Mod. Phys. **94**, 025005 (2022).

[63] E. A. Martinez, C. A. Muschik, P. Schindler, D. Nigg, A. Erhard, M. Heyl, P. Hauke, M. Dalmonte, T. Monz, P. Zoller, and R. Blatt, Real-time dynamics of lattice gauge theories with a few-qubit quantum computer, Nature (London) **534**, 516 (2016).

[64] N. Klco, E. F. Dumitrescu, A. J. McCaskey, T. D. Morris, R. C. Pooser, M. Sanz, E. Solano, P. Lougovski, and M. J. Savage, Quantum-classical computation of Schwinger model dynamics using quantum computers, Phys. Rev. A **98**, 032331 (2018).

[65] N. H. Nguyen, M. C. Tran, Y. Zhu, A. M. Green, C. H. Alderete, Z. Davoudi, and N. M. Linke, Digital quantum simulation of the Schwinger model and symmetry protection with trapped ions, PRX Quantum **3**, 020324 (2022).

[66] N. Mueller, J. A. Carolan, A. Connelly, Z. Davoudi, E. F. Dumitrescu, and K. Yeter-Aydeniz, Quantum computation of dynamical quantum phase transitions and entanglement tomography in a lattice gauge theory, PRX Quantum **4**, 030323 (2023).

[67] B. Chakraborty, M. Honda, T. Izubuchi, Y. Kikuchi, and A. Tomiya, Classically emulated digital quantum simulation of the Schwinger model with a topological term via adiabatic state preparation, Phys. Rev. D **105**, 094503 (2022).

[68] W. A. de Jong, K. Lee, J. Mulligan, M. Płoskoń, F. Ringer, and X. Yao, Quantum simulation of nonequilibrium dynamics and thermalization in the Schwinger model, Phys. Rev. D **106**, 054508 (2022).

[69] A. F. Shaw, P. Lougovski, J. R. Stryker, and N. Wiebe, Quantum algorithms for simulating the lattice Schwinger model, Quantum **4**, 306 (2020).

[70] A. Kan and Y. Nam, Lattice quantum chromodynamics and electrodynamics on a universal quantum computer, arXiv:2107.12769.

[71] Z.-Y. Zhou, G.-X. Su, J. C. Halimeh, R. Ott, H. Sun, P. Hauke, B. Yang, Z.-S. Yuan, J. Berges, and J.-W. Pan, Thermalization dynamics of a gauge theory on a quantum simulator, Science **377**, 311 (2022).

[72] B. Yang, H. Sun, R. Ott, H.-Y. Wang, T. V. Zache, J. C. Halimeh, Z.-S. Yuan, P. Hauke, and J.-W. Pan, Observation of gauge invariance in a 71-site Bose–Hubbard quantum simulator, Nature (London) **587**, 392 (2020).

[73] A. Mil, T. V. Zache, A. Hegde, A. Xia, R. P. Bhatt, M. K. Oberthaler, P. Hauke, J. Berges, and F. Jendrzejewski, A scalable realization of local U(1) gauge invariance in cold atomic mixtures, Science **367**, 1128 (2020).

[74] D. Banerjee, M. Dalmonte, M. Müller, E. Rico, P. Stebler, U.-J. Wiese, and P. Zoller, Atomic quantum simulation of dynamical gauge fields coupled to fermionic matter: From string breaking to evolution after a quench, Phys. Rev. Lett. **109**, 175302 (2012).

[75] P. Hauke, D. Marcos, M. Dalmonte, and P. Zoller, Quantum simulation of a lattice Schwinger model in a chain of trapped ions, Phys. Rev. X **3**, 041018 (2013).

[76] U.-J. Wiese, Ultracold quantum gases and lattice systems: Quantum simulation of lattice gauge theories, Ann. Phys. (Amsterdam) **525**, 777 (2013).

[77] E. Zohar, J. I. Cirac, and B. Reznik, Quantum simulations of lattice gauge theories using ultracold atoms in optical lattices, Rep. Prog. Phys. **79**, 014401 (2015).

[78] D. Yang, G. S. Giri, M. Johanning, C. Wunderlich, P. Zoller, and P. Hauke, Analog quantum simulation of $(1+1)$-dimensional lattice QED with trapped ions, Phys. Rev. A **94**, 052321 (2016).

[79] Z. Davoudi, M. Hafezi, C. Monroe, G. Pagano, A. Seif, and A. Shaw, Towards analog quantum simulations of lattice gauge theories with trapped ions, Phys. Rev. Res. **2**, 023015 (2020).

[80] D. Luo, J. Shen, M. Highman, B. K. Clark, B. DeMarco, A. X. El-Khadra, and B. Gadway, Framework for simulating gauge theories with dipolar spin systems, Phys. Rev. A **102**, 032617 (2020).

[81] S. Notarnicola, M. Collura, and S. Montangero, Real-time-dynamics quantum simulation of $(1+1)$-dimensional lattice QED with Rydberg atoms, Phys. Rev. Res. **2**, 013288 (2020).

[82] F. M. Surace, P. P. Mazza, G. Giudici, A. Lerose, A. Gambassi, and M. Dalmonte, Lattice gauge theories and string dynamics in Rydberg atom quantum simulators, Phys. Rev. X **10**, 021041 (2020).

[83] Z. Davoudi, N. M. Linke, and G. Pagano, Toward simulating quantum field theories with controlled phonon-ion dynamics: A hybrid analog-digital approach, Phys. Rev. Res. **3**, 043072 (2021).

[84] B. Andrade, Z. Davoudi, T. Graß, M. Hafezi, G. Pagano, and A. Seif, Engineering an effective three-spin Hamiltonian in trapped-ion systems for applications in quantum simulation, Quantum Sci. Technol. **7**, 034001 (2022).

[85] D. Marcos, P. Rabl, E. Rico, and P. Zoller, Superconducting circuits for quantum simulation of dynamical gauge fields, Phys. Rev. Lett. **111**, 110504 (2013).

[86] J. C. Halimeh, I. P. McCulloch, B. Yang, and P. Hauke, Tuning the topological θ-angle in cold-atom quantum simulators of gauge theories, PRX Quantum **3**, 040316 (2022).

[87] J. Osborne, B. Yang, I. P. McCulloch, P. Hauke, and J. C. Halimeh, Spin-S U(1) quantum link models with dynamical matter on a quantum simulator, arXiv:2305.06368.

[88] W.-Y. Zhang, Y. Liu, Y. Cheng, M.-G. He, H.-Y. Wang, T.-Y. Wang, Z.-H. Zhu, G.-X. Su, Z.-Y. Zhou, Y.-G. Zheng, H. Sun, B. Yang, P. Hauke, W. Zheng, J. C. Halimeh *et al.*, Observation of microscopic confinement dynamics by a tunable topological θ-angle, arXiv:2306.11794.

[89] L. Vanderstraeten, J. Haegeman, and F. Verstraete, Tangent-space methods for uniform matrix product states, SciPost Phys. Lect. Notes **7** (2019).

[90] J. Berges, S. Floerchinger, and R. Venugopalan, Thermal excitation spectrum from entanglement in an expanding quantum string, Phys. Lett. B **778**, 442 (2018).

[91] J. Berges, S. Floerchinger, and R. Venugopalan, Dynamics of entanglement in expanding quantum fields, J. High Energy Phys. 04 (2018) 145.

[92] D. E. Kharzeev and E. M. Levin, Deep inelastic scattering as a probe of entanglement, Phys. Rev. D **95**, 114008 (2017).

[93] Y. Hagiwara, Y. Hatta, B.-W. Xiao, and F. Yuan, Classical and quantum entropy of parton distributions, Phys. Rev. D **97**, 094029 (2018).

[94] A. Kovner, M. Lublinsky, and M. Serino, Entanglement entropy, entropy production and time evolution in high energy QCD, Phys. Lett. B **792**, 4 (2019).

[95] S. R. Beane, D. B. Kaplan, N. Klco, and M. J. Savage, Entanglement suppression and emergent symmetries of strong interactions, Phys. Rev. Lett. **122**, 102001 (2019).

[96] S. R. Beane and P. J. Ehlers, Chiral symmetry breaking, entanglement, and the nucleon spin decomposition, Mod. Phys. Lett. A **35**, 2050048 (2020).

[97] S. R. Beane and R. C. Farrell, Geometry and entanglement in the scattering matrix, Ann. Phys. (Amsterdam) **433**, 168581 (2021).

[98] A. Kruckenhauser, R. van Bijnen, T. V. Zache, M. Di Liberto, and P. Zoller, High-dimensional SO(4)-symmetric Rydberg manifolds for quantum simulation, Quantum Sci. Technol. **8**, 015020 (2023).

[99] P. Forn-Díaz, L. Lamata, E. Rico, J. Kono, and E. Solano, Ultrastrong coupling regimes of light-matter interaction, Rev. Mod. Phys. **91**, 025005 (2019).

[100] A. Frisk Kockum, A. Miranowicz, S. De Liberato, S. Savasta, and F. Nori, Ultrastrong coupling between light and matter, Nat. Rev. Phys. **1**, 19 (2019).

[101] S. Coleman, R. Jackiw, and L. Susskind, Charge shielding and quark confinement in the massive schwinger model, Ann. Phys. (N.Y.) **93**, 267 (1975).

[102] S. Coleman, More about the massive Schwinger model, Ann. Phys. (N.Y.) **101**, 239 (1976).

[103] See Supplemental Material at http://link.aps.org/supplemental/10.1103/PhysRevLett.132.091903 for additional details concerning the general massive Thirring-Schwinger model, its experimental implementation with circuit QED, experimental wave-packet preparation scheme, the derivation of the effective quark-antiquark Hamiltonian, and details on the numerical methods. Includes Refs. [104–112].

[104] R. F. Dashen, B. Hasslacher, and A. Neveu, Particle spectrum in model field theories from semiclassical functional integral techniques, Phys. Rev. D **11**, 3424 (1975).

[105] A. B. Zamolodchikov and A. B. Zamolodchikov, Factorized S-matrices in two dimensions as the exact solutions of certain relativistic quantum field theory models, Ann. Phys. (N.Y.) **120**, 253 (1979).

[106] D. J. Griffiths and D. F. Schroeter, *Introduction to Quantum Mechanics*, 3rd ed. (Cambridge University Press, Cambridge, 2018).

[107] M. Peruzzo, F. Hassani, G. Szep, A. Trioni, E. Redchenko, M. Žemlička, and J. M. Fink, Geometric superinductance qubits: Controlling phase delocalization across a single Josephson junction, PRX Quantum **2**, 040341 (2021).

[108] S. E. Rasmussen, K. S. Christensen, S. P. Pedersen, L. B. Kristensen, T. Baekkegaard, N. J. S. Loft, and N. T. Zinner, Superconducting circuit companion: An introduction with worked examples, Phys. Rev. Appl. **10**, 040204 (2021).

[109] I. Siddiqi, Engineering high-coherence superconducting qubits, Nat. Rev. Mater. **6**, 875 (2021).

[110] N. Y. Yao, C. R. Laumann, A. V. Gorshkov, H. Weimer, L. Jiang, J. I. Cirac, P. Zoller, and M. D. Lukin, Topologically protected quantum state transfer in a chiral spin liquid, Nat. Commun. **4**, 1585 (2013).

[111] L. Magazzù, P. Forn-Díaz, R. Belyansky, J.-L. Orgiazzi, M. A. Yurtalan, M. R. Otto, A. Lupascu, C. M. Wilson, and M. Grifoni, Probing the strongly driven spin-boson model in a superconducting quantum circuit, Nat. Commun. **9**, 1403 (2018).

[112] J. Haegeman, C. Lubich, I. Oseledets, B. Vandereycken, and F. Verstraete, Unifying time evolution and optimization with matrix product states, Phys. Rev. B **94**, 165116 (2016).

[113] S. Coleman, Quantum sine-Gordon equation as the massive Thirring model, Phys. Rev. D **11**, 2088 (1975).

[114] H. Ohata, Monte Carlo study of Schwinger model without the sign problem, J. High Energy Phys. 12 (2023) 007.

[115] T. V. Zache, M. Van Damme, J. C. Halimeh, P. Hauke, and D. Banerjee, Toward the continuum limit of a $(1+1)$D quantum link Schwinger model, Phys. Rev. D **106**, L091502 (2022).

[116] R. Shankar and G. Murthy, Deconfinement in $d = 1$: Asymptotic and half-asymptotic particles, Phys. Rev. B **72**, 224414 (2005).

[117] V. Zauner-Stauber, L. Vanderstraeten, M. T. Fishman, F. Verstraete, and J. Haegeman, Variational optimization algorithms for uniform matrix product states, Phys. Rev. B **97**, 045145 (2018).

[118] J. Haegeman, B. Pirvu, D. J. Weir, J. I. Cirac, T. J. Osborne, H. Verschelde, and F. Verstraete, Variational matrix product ansatz for dispersion relations, Phys. Rev. B **85**, 100408(R) (2012).

[119] J. Haegeman, S. Michalakis, B. Nachtergaele, T. J. Osborne, N. Schuch, and F. Verstraete, Elementary excitations in gapped quantum spin systems, Phys. Rev. Lett. **111**, 080401 (2013).

[120] A. Milsted, J. Haegeman, T. J. Osborne, and F. Verstraete, Variational matrix product ansatz for nonuniform dynamics in the thermodynamic limit, Phys. Rev. B **88**, 155116 (2013).

[121] H. N. Phien, G. Vidal, and I. P. McCulloch, Dynamical windows for real-time evolution with matrix product states, Phys. Rev. B **88**, 035103 (2013).

[122] V. Zauner, M. Ganahl, H. G. Evertz, and T. Nishino, Time evolution within a comoving window: Scaling of signal fronts and magnetization plateaus after a local quench in quantum spin chains, J. Phys. Condens. Matter **27**, 425602 (2015).

[123] H. J. Rothe, K. D. Rothe, and J. A. Swieca, Screening versus confinement, Phys. Rev. D **19**, 3020 (1979).

[124] $S_{\mathrm{vN}}(x,t) = -\mathrm{tr}(\rho_{>x}(t)\ln\rho_{>x}(t))$ with $\rho_{>x}(t)$ being the reduced density matrix for sites $y > x$.

[125] Projecting the state on four widely separated quarks basis states resulted in a negligible contribution. This suggests that the four particles are not sufficiently spatially separated.

[126] S. Coleman, Fate of the false vacuum: Semiclassical theory, Phys. Rev. D **15**, 2929 (1977).

[127] C. G. Callan and S. Coleman, Fate of the false vacuum. II. First quantum corrections, Phys. Rev. D **16**, 1762 (1977).

[128] F. Hebenstreit, J. Berges, and D. Gelfand, Real-time dynamics of string breaking, Phys. Rev. Lett. **111**, 201601 (2013).

[129] We verified that the missing wave-function weight is not accounted for by three or four widely separated particle basis states.

[130] A. B. Özgüler, V. E. Manucharyan, and M. G. Vavilov, Excitation dynamics in inductively coupled fluxonium circuits, arXiv:2104.03300.
[131] A. Blais, A. L. Grimsmo, S. M. Girvin, and A. Wallraff, Circuit quantum electrodynamics, Rev. Mod. Phys. **93**, 025005 (2021).
[132] J. Fröhlich and E. Seiler, The massive Thirring-Schwinger model (QED_2): Convergence of perturbation theory and particle structure, Helv. Phys. Acta **49**, 889 (1976).
[133] X. Zhang, E. Kim, D. K. Mark, S. Choi, and O. Painter, A superconducting quantum simulator based on a photonic-bandgap metamaterial, Science **379**, 278 (2023).
[134] P. Forn-Díaz, J. J. García-Ripoll, B. Peropadre, J.-L. Orgiazzi, M. A. Yurtalan, R. Belyansky, C. M. Wilson, and A. Lupascu, Ultrastrong coupling of a single artificial atom to an electromagnetic continuum in the nonperturbative regime, Nat. Phys. **13**, 39 (2017).
[135] A. Vrajitoarea, R. Belyansky, R. Lundgren, S. Whitsitt, A. V. Gorshkov, and A. A. Houck, Ultrastrong light-matter interaction in a photonic crystal, arXiv:2209.14972.
[136] L. Vanderstraeten, J. Haegeman, T. J. Osborne, and F. Verstraete, S matrix from matrix product states, Phys. Rev. Lett. **112**, 257202 (2014).
[137] R. Verdel, G.-Y. Zhu, and M. Heyl, Dynamical localization transition of string breaking in quantum spin chains, Phys. Rev. Lett. **131**, 230402 (2023).
[138] T. V. Zache, N. Mueller, J. T. Schneider, F. Jendrzejewski, J. Berges, and P. Hauke, Dynamical topological transitions in the massive Schwinger model with a θ term, Phys. Rev. Lett. **122**, 050403 (2019).
[139] J.-Y. Desaules, D. Banerjee, A. Hudomal, Z. Papić, A. Sen, and J. C. Halimeh, Weak ergodicity breaking in the Schwinger model, Phys. Rev. B **107**, L201105 (2023).
[140] J.-Y. Desaules, A. Hudomal, D. Banerjee, A. Sen, Z. Papić, and J. C. Halimeh, Prominent quantum many-body scars in a truncated Schwinger model, Phys. Rev. B **107**, 205112 (2023).
[141] Z. Tian, J. Jing, and A. Dragan, Analog cosmological particle generation in a superconducting circuit, Phys. Rev. D **95**, 125003 (2017).
[142] L. García-Álvarez, J. Casanova, A. Mezzacapo, I. L. Egusquiza, L. Lamata, G. Romero, and E. Solano, Fermion-fermion scattering in quantum field theory with superconducting circuits, Phys. Rev. Lett. **114**, 070502 (2015).
[143] A. Roy, D. Schuricht, J. Hauschild, F. Pollmann, and H. Saleur, The quantum sine-Gordon model with quantum circuits, Nucl. Phys. **B968**, 115445 (2021).
[144] A. Roy and S. Lukyanov, Soliton confinement in a quantum circuit, Nat. Commun. **14**, 7433 (2023).
[145] M. C. Bañuls, K. Cichy, J. I. Cirac, K. Jansen, and S. Kühn, Density induced phase transitions in the Schwinger model: A study with matrix product states, Phys. Rev. Lett. **118**, 071601 (2017).
[146] https://github.com/maartenvd/MPSKit.jl.
[147] http://hpcc.umd.edu.